



Gas phase pyrolysis synthesis of carbon nanotubes at high temperature



Guangfeng Hou ^{a,*}, Devika Chauhan ^b, Vianessa Ng ^a, Chenhao Xu ^a, Zhangzhang Yin ^a, Michael Paine ^a, Ruitao Su ^c, Vesselin Shanov ^a, David Mast ^d, Mark Schulz ^{a,*}, Yijun Liu ^a

^a Department of Mechanical and Materials Engineering, University of Cincinnati, OH 45221, United States

^b Department of Aerospace Engineering and Engineering Mechanics, University of Cincinnati, OH 45221, United States

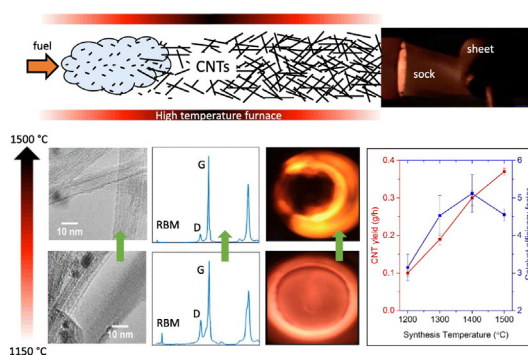
^c Department of Mechanical Engineering, University of Minnesota, MN 55455, United States

^d Department of Physics, University of Cincinnati, OH 45221, United States

HIGHLIGHTS

- High-temperature synthesis of CNTs in gas phase pyrolysis method has been investigated.
- The CNTs transform from single-walled to multi-walled, with an increase of amorphous impurities at elevated temperature.
- The CNT quality increases at higher temperature, indicated by a higher Raman I_G/I_D ratio.
- The catalyst efficiency is highest at 1400 °C with 1 g Fe producing 5.1 g CNT.

GRAPHICAL ABSTRACT



ARTICLE INFO

Article history:

Received 27 April 2017

Received in revised form 28 June 2017

Accepted 29 June 2017

Available online 30 June 2017

ABSTRACT

In this study, carbon nanotubes were synthesized at high temperature (1150–1500 °C) using the substrate-free gas phase pyrolysis method. The CNT sock morphology, CNT structure, impurity, process yield and growth efficiency at high temperatures were investigated. It was found that the CNTs transform from single-walled to multi-walled nanotubes at elevated temperature. The amount of amorphous impurities increases with higher temperature, possibly due to an increased non-catalytic decomposition of hydrocarbons. However the CNT quality increases, as indicated by a higher Raman spectroscopy I_G/I_D ratio. The process yield increase by two folds at higher temperature (1500 °C) compared to a lower temperature (1200 °C), but the catalyst efficiency is highest at 1400 °C with 1 g Fe producing 5.1 g CNT. The calculated carbon conversion rate is lower than 4%. The CNT growth is not limited by the availability of carbon around the catalyst, instead of by the availability of active catalyst particles. Based on a pristine CNT sheet, the measured electrical conductivity is highest at 1400 °C, due to a balance between impurities and CNT quality. The tensile strength of the CNT sheet increases with the temperature, possibly because of the “gluing” effect of the carbonaceous impurities.

© 2017 Elsevier Ltd. All rights reserved.

1. Introduction

Carbon nanotubes (CNTs) have found applications in various engineering fields such as electronics [1], composites [2,3], biosensors [4], and energy storage [5]. There are large efforts toward their commercialization [6–8]. Among different CNT synthesis methods, gas phase

* Corresponding authors.

E-mail addresses: hougg@mail.uc.edu (G. Hou), Mark.J.Schulz@uc.edu (M. Schulz).

pyrolysis method (floating catalyst method) has been widely used both in academia [9–15] and industry [16,17]. It holds high promise for large scale commercialization of nano material sheet and yarn. In the gas phase pyrolysis synthesis method, relatively lower temperature (500–1000 °C) is used to produce multi-walled nanotube (MWNT) arrays on silica substrates or on the reactor walls [18,19]. Whereas higher temperature (1150–1500 °C) is usually employed for aerogel-like CNT sock (cylindrical web of nanotubes) production without substrate, which is a critical link directly bridging the nanoscale CNTs with macroscale CNT yarn and sheets [20,21]. For sock formation, the high synthesis temperature could be critical for fast growth rate and long CNTs, which helps keep the CNTs away from the reactor wall and form an entangled aerogel-like sock [22].

It is generally accepted that high-temperature synthesis methods produce CNTs of better quality. MWNTs produced from the chemical vapor deposition (CVD) method at a relatively lower temperature of 600–1000 °C contain more defects than nanotubes produced from other high-temperature methods because the lower temperature doesn't allow any structural rearrangements [23]. For the arc discharge method, the high temperature plasma can provide in-situ defect healing effect [24]. Guo et al. [25] found that in the laser ablation process the CNT yield and quality of MWNTs decline as the oven temperature decreases from 1200 °C to 900 °C, and defects became increasingly prevalent.

There are several studies of the temperature effect on the substrate-based gas phase pyrolysis method for MWNT array production. The synthesis temperature influences the CNT growth rate, the size of the catalyst particle and thus the diameter of the CNTs. The diameter of the CNT was found to increase with higher synthesis temperature [26]. The average CNT diameter may also change nonlinearly with temperature. For example it has been observed that the CNT diameter increases from 550 °C to 850 °C, and then decreases till 900 °C [27]. Kim et al. [28] observed that the CNT diameter stays constant at synthesis temperature from 600 to 900 °C. Xiang et al. [29] found that the CNT growth rate is highest at moderate synthesis temperature (820 °C), which decreases at higher temperatures. These varying results may originate from the interaction of the catalyst particle with the substrate, where catalyst coalescence and diffusion occurs. For substrate-free gas phase pyrolysis process, there should be more definitive results due to the absence of catalyst-substrate interaction.

Despite the wide use of substrate-free gas phase pyrolysis method for synthesizing aerogel-like CNT sock, there is little study at the higher temperature end (>1300 °C). Most of the studies operate at synthesis temperature around 1250 °C or lower [30–35], although a higher temperature is mentioned possible for successful CNT synthesis [36–39]. There is no detailed report regarding temperature effect on the aerogel-like sock synthesis method, especially at higher temperatures (>1300 °C). In this study, we systematically investigated the effect of synthesis temperature (1150 °C to 1500 °C) on the aerogel-like sock system, including sock formation and morphology, CNT growth efficiency, quality of the synthesized CNTs, properties of macroscale sheet, and process yield. The obtained results provide insights on the process mechanism and scale-up capabilities.

2. CNT synthesis and sample characterization methods

The details of the CNT synthesis setup can be found in our previous publication [20]. In the experiment the feedstock is composed of methanol (90 vol%, Fisher Scientific), hexane (10 vol%, Fisher Scientific), ferrocene (1 wt%, Sigma-Aldrich) and thiophene (0.3 vol%, Sigma-Aldrich). This feedstock is injected into the high temperature furnace (Fig. 1) at a rate of 32 ml/h, and argon is used as carrier gas at 1200 sccm. The aerogel-like CNT sock is synthesized at atmospheric pressure inside a ceramic tube and subsequently collected on a drum inside a harvest box to produce the CNT sheet.

The samples were characterized using a Renishaw in via Raman spectroscope, with an argon laser of 514 nm wavelength and R-type laser of 785 nm wavelength. The Raman data was collected on multi spots of the as-prepared CNT samples, >20 scans are obtained for each sample and the average is used for the data analysis. A Netzsch STA409 thermal gravimetric analysis (TGA) analyzer has been used to characterize the samples. As-prepared CNT samples with the weight of above 10 mg are used in the experiment, which were heated up from room temperature to 1000 °C at a rate of 5 °C/min in 100 ml/min of air. An FEI CM20 transmission electron microscope (TEM) and FEI XL30 scanning electron microscope (SEM) have been used for imaging the samples. The electrical conductivity has been measured using a Jandel RM3000 four probe system. The tensile strength of CNT sheet was determined using an Instron machine, with a gauge length of 23.5 mm, and width of 2 mm at 1 mm/s extension rate.

3. Results and discussion

3.1. CNT sock morphology

We observed that the CNT sock could not form at a temperature of 1150 °C. There are unorganized CNT webs formed inside the reactor at 1150 °C, but the aerogel-like sock could not be assembled. For our reactor, the sock could form in the temperature range from 1200 °C to 1500 °C. The highest temperature is limited by the capability of the furnace. The aerogel-like sock is less stable at 1200 °C, which occasionally sticks to the wall of the ceramic tube. With the increase of synthesis temperature, the sock becomes darker and flows out more smoothly (Fig. 2). This is due to the increased amount of CNTs synthesized at a higher temperature, which can be qualitatively characterized by the process yield. The process yield and efficiency will be discussed further in a later section.

3.2. CNT structure

The synthesized CNTs are a combination of single-walled carbon nanotubes (SWNTs) and multi-walled carbon nanotubes (MWNTs). At higher temperature, there is an increase of CNT diameter, indicated by more MWNTs in the TEM images (Fig. S1). Due to the limitation of the TEM machine, the exact diameter is beyond our system's capability. The transition from SWNT to MWNTs can be further confirmed by the reduced radial breathing mode (RBM) signals in Raman spectra. At

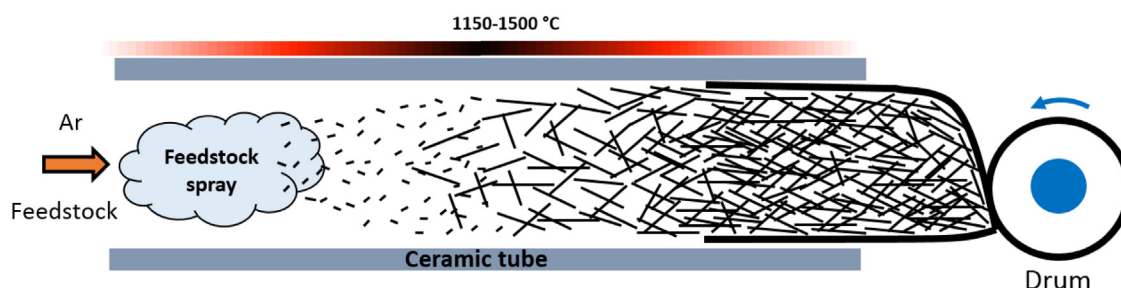


Fig. 1. Schematic of the experimental setup.

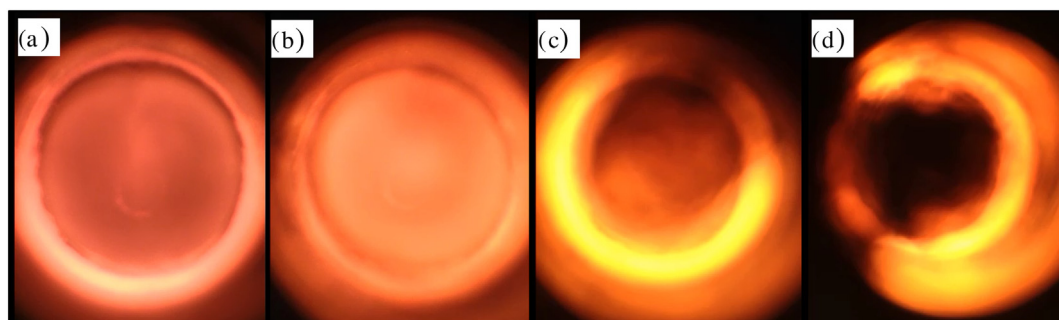


Fig. 2. Morphologies of CNT sock at different temperatures: (a) 1200 °C, less amount of CNTs and thin aerogel-like sock; (b) 1300 °C; (c) 1400 °C; (d) 1500 °C, increased amount of CNTs and dense aerogel-like sock.

higher temperature (> 1300 °C) the RBM signals drop significantly (Fig. 3), which indicates the reduction of the SWNTs percentage in the sample. The SWNT diameter is calculated using the RBM frequencies (see Section 1 of Supporting information). There is one dominant diameter (0.86 nm) in the 514 nm spectra and two dominant diameters (0.83 nm and 0.95 nm) in the 785 nm spectra. Several minor peaks also exist, which have an intensity much smaller than the dominant peaks.

The transition from SWNTs to MWNTs while increasing the synthesis temperature could be caused by the larger catalyst particles at a higher temperature. Iron atoms are released from ferrocene decomposition. Their diffusion and coagulation determine the size of the catalyst particle. At higher temperatures, the catalyst particles have a higher collision frequency [40], which can cause the increase of the average catalyst diameter.

3.3. CNT purity and quality

The purity of different CNT samples can be roughly compared under SEM (Fig. S2 and S3). At higher temperature (> 1300 °C), the amount of large cluster impurities (~350 nm) reduces, meanwhile there is an increased number of small impurities (~50 nm). These impurities are believed to be catalyst particles with amorphous carbon or curly MWNTs. The impurity level can be further evaluated by TGA analysis. Different burning events can be observed from the TGA curves (Fig. 4). The amorphous impurities burn out first at a temperature below 400 °C, followed by two main oxidation events at ~520 °C and ~660 °C. These two events possibly correspond to SWNTs and MWNTs oxidation respectively. The separated burning events for two types of CNTs were also observed by another group [22]. Accurate determination of the percentage of SWNTs and MWNTs is challenging because the oxidation events happen in a range and different burning events overlap. The amount of

amorphous impurities increases from 2.33% at 1200 °C to 8.56% at 1500 °C (Table S3). This can be caused by the non-catalytic decomposition of hydrocarbons at elevated temperature, which introduces more amorphous impurities as by-products.

From the Raman spectra (Fig. 5), several conclusions can be made. There is an obvious decrease of the D peak at a higher temperature, indicating a decrease in defects and graphitic impurities. In consideration of the larger amount of amorphous impurities at a higher temperature, there should be a large increase of CNT quality in order to mask the influence of the amorphous impurities. The I_G/I_D ratio almost increases by >200%, from 1150 °C to 1500 °C (Fig. 6). This shows that CNTs of better quality with fewer defects can be obtained from higher temperature. The full width at half maximum (FWHM) of the G peak decrease with increasing temperature (Table S2), due to the increased uniformity of the synthesized high-quality material.

The electron microscopy imaging, Raman, and TGA results reveal that at a higher temperature, amorphous impurities increase, yet the CNTs have better quality in graphitic structure. Moreover there is a partial transition from SWNTs to MWNTs at elevated synthesis temperature.

3.4. Growth efficiency and process yield

The collected CNT sock is composed of amorphous impurities, CNTs and catalyst particles. The CNT mass in the sock can be estimated by subtracting the mass of the amorphous impurities and the residual catalyst. With these experimental data, the carbon conversion rate ($C_{CNT}/C_{feedstock}$) and iron conversion rate ($Fe_{CNT}/Fe_{feedstock}$) can be calculated (Table S5). The carbon conversion rate is considerably low at all temperature levels. Most of the carbon (>96%) escaped from the reactor in the form of by-product carbonaceous gas along with the carrier gas. The carbon conversion rate increases from 0.91% at 1200 °C to 3.53% at 1500 °C

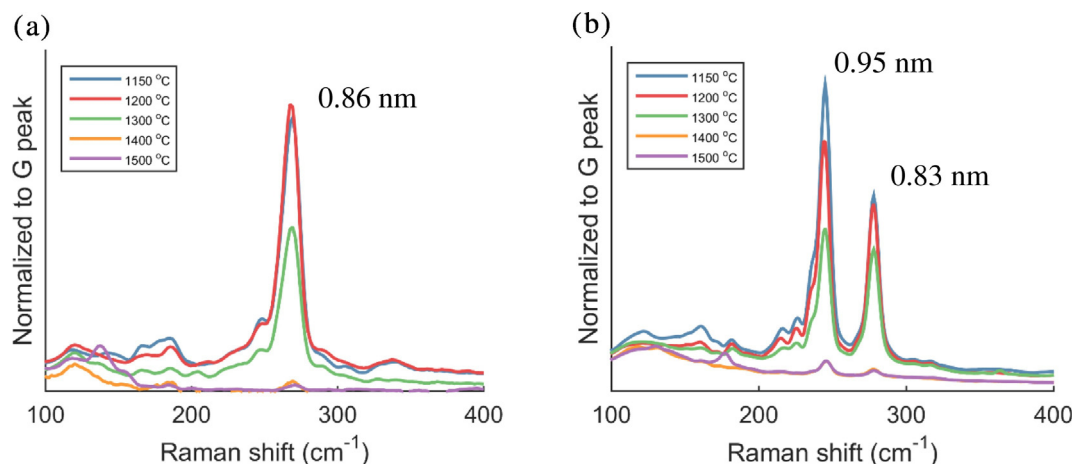


Fig. 3. RBM peaks with calculated SWNT diameter. (a) 514 nm laser, and (b) 785 nm laser.

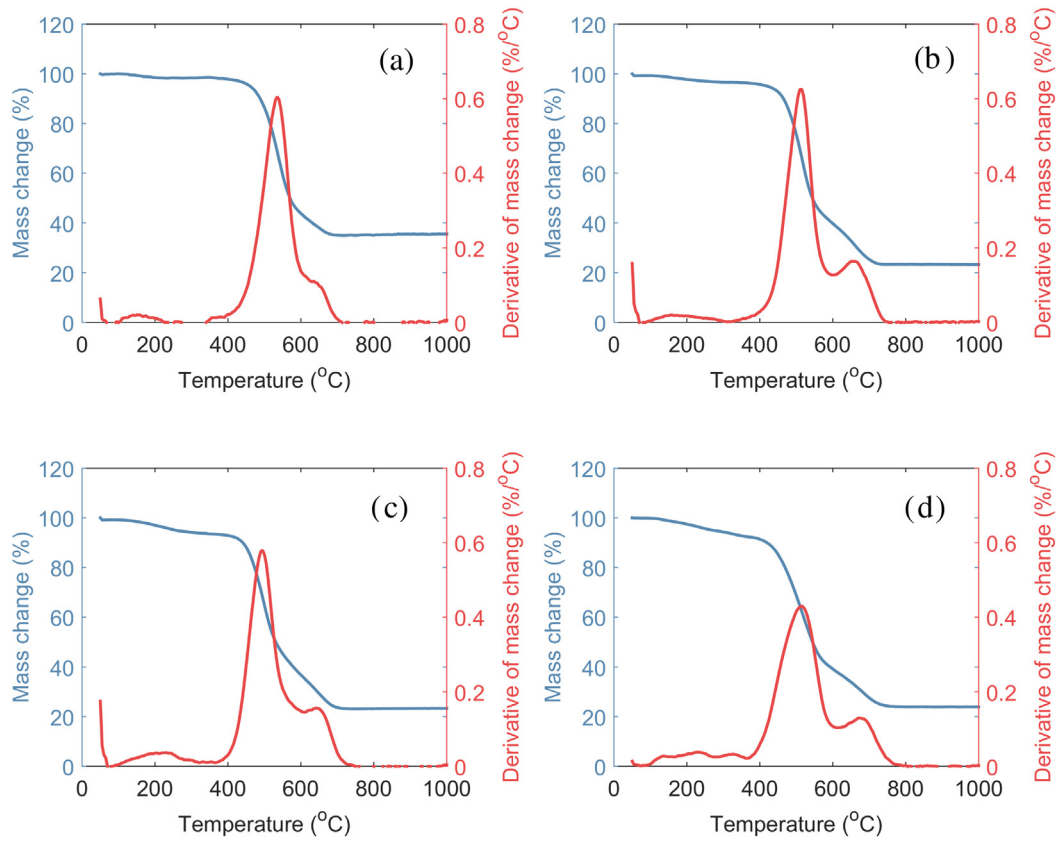


Fig. 4. Representative TGA curves of CNT synthesized at different temperatures: (a) 1200 °C; (b) 1300 °C; (c) 1400 °C; (d) 1500 °C.

(Fig. 7). A relatively lower temperature (<1000 °C) has been used in substrate-based gas phase pyrolysis methods to synthesize MWNT array [18,19], which indicates the temperature of 1200 °C is high enough to decompose the hydrocarbon, releasing enough carbon for CNT growth. The CNT growth is not limited by the availability of carbon around the catalyst, instead it is limited by the number of active catalyst particles. The increased carbon conversion rate at higher temperature should be due to more active catalyst particles or faster CNT growth rate, which converts more carbon into CNTs.

Looking at the iron conversion rate, it increases significantly from 31.77% at 1200 °C to 85.04% at 1500 °C (Fig. 7). This means a significant amount of iron particles are “lost” during the synthesis and don’t end up in the sock, especially at a lower temperature. There are two

possibilities, the catalyst particles either deposit on the wall of the ceramic tube or escape from the reactor with the carrier gas. Indeed we observed a large amount of catalyst particles coating on the reactor wall after heating the reactor in air to clean the ceramic tube (Fig. S5). The deposition doesn’t occur in the middle high-temperature growth zone, instead the catalyst deposits on the low-temperature inlet and outlet regions. This might be caused by a thermophoretic repulsion force which prevents the nanoparticles and CNTs from depositing on the reactor wall in the high-temperature synthesis zone [41]. The catalyst particles can also be transported out along with the carrier gas, without being incorporated inside the sock. We have observed CNT webs attached to the side walls of the harvest box under stable sock formation, which indicates that smaller CNTs and thus catalyst particles

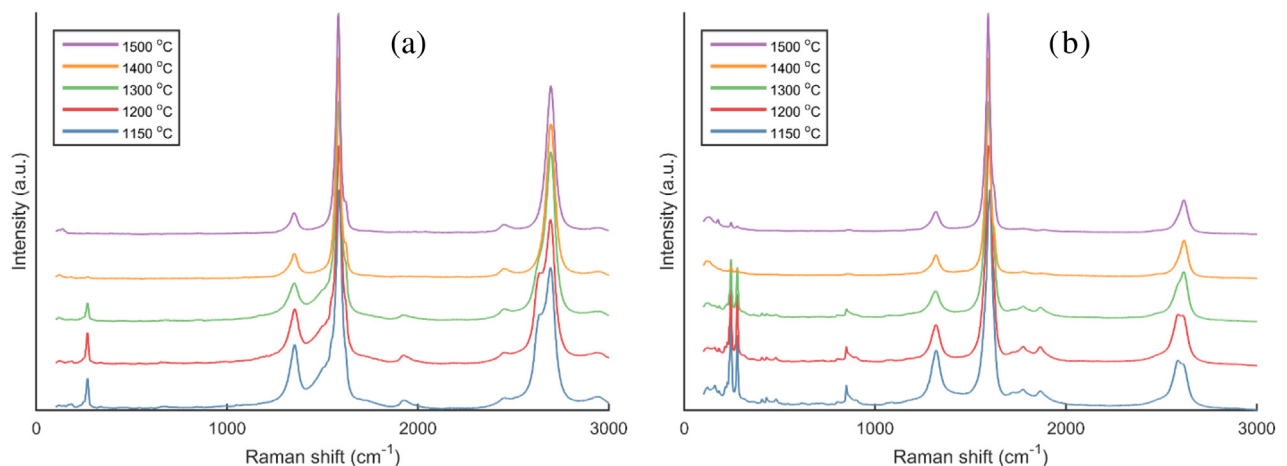


Fig. 5. Raman plot of samples synthesized at different temperatures: (a) 514 nm laser data normalized to the G peak; (b) 785 nm laser data normalized to the G peak.

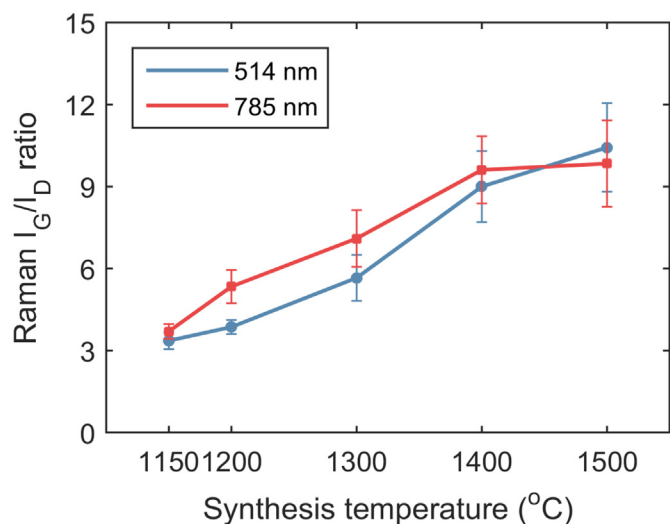


Fig. 6. Raman I_G/I_D ratio at different temperatures.

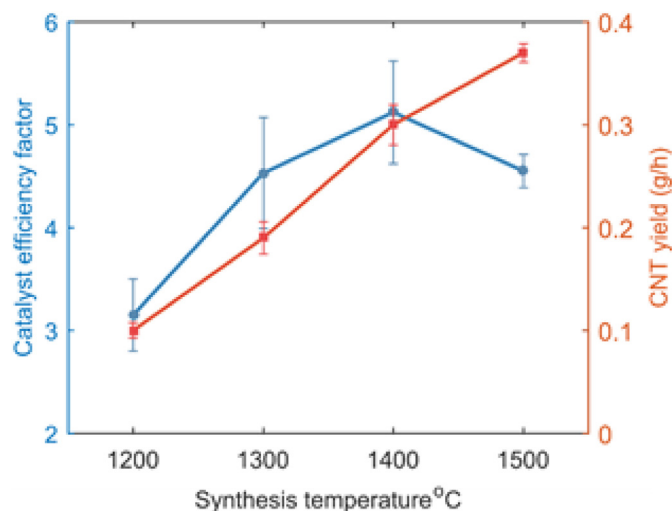


Fig. 8. CNT yield and catalyst efficiency factor (carbon output per unit mass Fe) at different synthesis temperatures.

can escape from the sock. Thus it is highly possible that small catalyst particles and short CNTs travel out of the reactor, either through the porous sock or more possibly through the gap between the sock and the reactor wall.

Accurately separating these two effects is difficult, however there is evidence that the particle escaping mechanism might dominate in our process. It has been shown that the catalyst deposition mainly happens around the inlet and outlet region of the reactor tube. The temperature change in these zones at different synthesis temperatures (1200 °C–1500 °C), is not expected to vary significantly due to the low thermal conductivity of the ceramic tube. There is no doubt the temperature around tube inlet and outlet will increase at higher temperature, but this increase is not able to explain the two thirds decrease of the lost iron at 1500 °C. Hence we conclude that the main reason for the higher iron conversion rate at increased temperature is due to fewer catalyst particles escaping the sock. The exact mechanism is not clear and needs further study, however we suggest that it is caused by more active catalyst particles and longer CNTs at a higher temperature. We have already observed that there is a transition from SWNTs to MWNTs at higher temperatures, which indicates the average catalyst particle size increases at elevated temperature. This shift of the catalyst size is believed to contribute to the greater amount of iron in the CNT sock. Another contributing factor is longer CNTs synthesized at a higher temperature. It is generally agreed that at higher temperature the hydrocarbon decomposition and CNT nucleation could happen at a higher rate, which leads to faster growth rate and longer CNTs in the aerogel-like CNT sock. With longer CNTs at higher temperatures, the sock

becomes denser and looks darker (Fig. 2). Thus shorter CNTs and inactive catalyst particles will have a lower chance of escaping the CNT sock. By using a linear and second order polynomial regression fit, a range between 1551 °C to 1605 °C is predicted as the threshold temperature at which the iron particles will be totally incorporated in the CNT growth (Fig. 7). In reality it is impossible to achieving 100% iron conversion rate, because there will always be a small amount of particles depositing on the wall or escaping the reactor.

It was observed that the CNT yield (g/h) is higher at elevated temperature, increasing from 0.10 g/h at 1200 °C to 0.37 g/h at 1500 °C (Fig. 8 and Table S4). Although the total iron from the feedstock stays unchanged, the yield almost increases linearly with temperature, which can be caused by either more CNTs or longer CNTs. At higher temperature there are more catalyst particles incorporated in the sock (Table S4), thus nucleating more CNTs. Meanwhile, higher molecular energy may activate a faster growth rate, leading to longer CNTs. Both effects are likely at a higher temperature, which together contribute to the greater yield.

Using the mass of the CNT and iron catalyst particles, the carbon output per unit mass of iron can be calculated (C_{CNT}/Fe_{sock}), which is defined as the catalyst efficiency factor. Initially the catalyst efficiency increases with higher temperature, which reaches the highest value at 1400 °C, where 1 g Fe nucleates 5.12 g CNTs. When the synthesis temperature increases to 1500 °C, the catalyst efficiency factor drops to 4.55. This decrease could be caused by the incorporation of shorter CNTs and inactive catalyst particles as discussed before, which lowers the ratio of the mass of CNT to the mass of the iron.

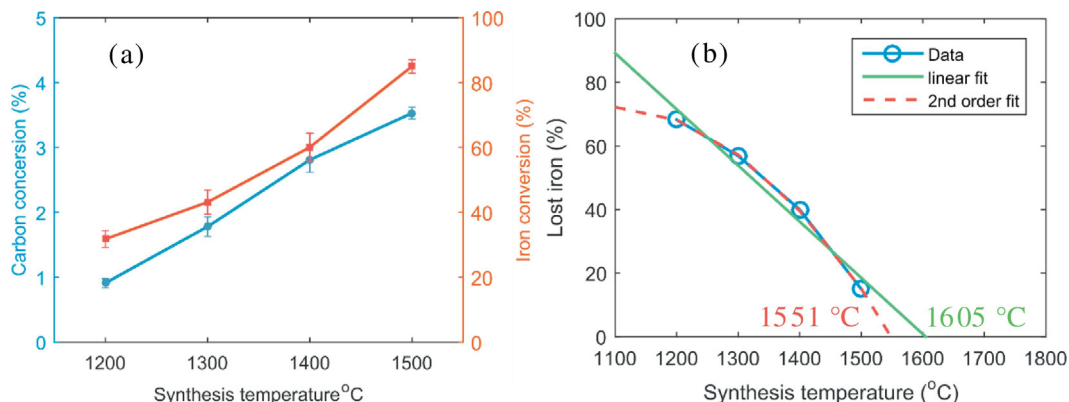


Fig. 7. Process efficiency: (a) Carbon (CNT) and iron conversion rate at different temperatures; (b) lost iron at different temperatures.

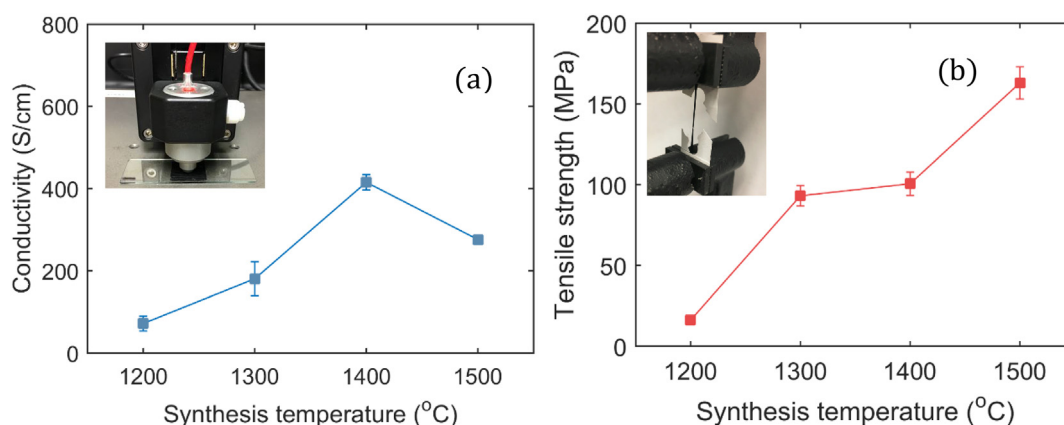


Fig. 9. CNT sheet properties at different temperatures: (a) conductivity, (b) tensile strength.

To better understand the process mechanism, an advanced model is needed to investigate the thermophoretic force and particle deposition. Moreover not all the iron catalyst inside the sock contribute to the CNT growth [9,36]. We speculate the percentage of iron inside the sock nucleating CNTs will vary at different temperatures. The total iron inside the sock has been used in our previous analysis. Though challenging, a more accurate estimation of the active iron percentage inside the sock at different synthesis conditions will provide better data to investigate the process mechanism.

3.5. Mechanical and electrical properties

CNT sheet samples are collected at different temperatures, which are used for mechanical strength and electrical conductivity measurement (Fig. 9). The conductivity of the CNT sheet is measured using a Jandel RM3000 linear four-probe sheet resistance measurement system with probe separation of 1 mm. All samples are densified using acetone to achieve same compactness level. Square samples of 20 mm by 20 mm have been used for measurement. The measured sheet resistance values have been converted to resistivity by multiplying the sample thickness. Based on the measurement results, the CNT sheet at 1400 °C has the highest conductivity. The electrical conductivity is related to the CNT quality and amount of impurities. A balance of CNT quality and impurity level at 1400 °C leads to the highest conductivity. Note that the catalyst efficiency factor is also highest at 1400 °C. This observation suggests that these two parameters are related to each other, although the exact mechanism needs further investigation. The tensile strength is affected by the CNT bundle strength and inter-bundle contacts, and it is found to increase with the synthesis temperature. The existence of amorphous impurities might have a large influence on the tensile strength. It is suggested the carbonaceous deposits can link the CNT bundles together, increasing the inter-bundle adhesion [42,43]. Considering the increase in the amount of amorphous impurities and a decrease of the large clusters at a higher temperature, we believe our results follow a similar mechanism where the carbonaceous impurities “glue” the CNT bundles together to enhance the inter-bundle sliding, which leads to higher tensile strength.

4. Conclusions

This study provides a detailed investigation of the synthesis of CNTs with substrate-free gas phase pyrolysis method at high temperatures. The CNTs were found to partially transform from SWNTs to MWNTs at elevated temperature. Even though the amount of amorphous impurities increases with temperature, the CNT quality improves in terms of reduced graphitic defects. From the process yield and efficiency analysis, it is found the CNT growth is limited by the availability of active catalyst particles, not by the availability of carbon around the catalyst. The

observed CNT structure and impurities have a different influence on the tensile strength and electrical conductivity. The CNT sheet has a highest electrical conductivity at 1400 °C, because of a balance between the impurity level and CNT quality. The tensile strength increases with the temperature, due to a dominant adhesion effect from the amorphous contents.

Acknowledgements

This work was supported the University of Cincinnati, College of Engineering under Associate Dean for Research Dr. Tim Keener, and ONR Award N00014-15-1-2473 under Program Manager Dr. Ignacio Perez. We thank Mark Haase for help in TGA measurement and Dr. David Lashmore from the University of New Hampshire for valuable discussions.

Appendix A. Supplementary data

Supplementary data to this article can be found online at <http://dx.doi.org/10.1016/j.matdes.2017.06.070>.

References

- [1] K. Chen, W. Gao, S. Emaminejad, D. Kiriya, H. Ota, H.Y.Y. Nyein, K. Takei, A. Javey, Printed carbon nanotube electronics and sensor systems, *Adv. Mater.* 28 (2016) 4397–4414.
- [2] Y. Song, D. Chauhan, G. Hou, X. Wen, M. Kattoura, C. Ryan, Carbon nanotube sheet reinforced laminated composites, *ASC 31st Tech. Conf. Williamsburg, VA*, 2016.
- [3] D. Chauhan, G. Hou, V. Ng, S. Chaudhary, M. Paine, K. Moinuddin, M. Rabiee, M. Cahay, N. Lalley, V. Shanov, D. Mast, Y. Liu, Z. Yin, Y. Song, M. Schulz, D.J. Leo, P.A. Tarazaga, Multifunctional Smart Composites With Integrated Carbon Nanotube Yarn and Sheet, 2017 1017205, <http://dx.doi.org/10.1117/12.2258563>.
- [4] G. Hou, L. Zhang, V. Ng, Z. Wu, M. Schulz, Review of recent advances in carbon nanotube biosensors based on field-effect transistors, *Nano Life* 6 (2016) 1642006, <http://dx.doi.org/10.1142/S179398441642006X>.
- [5] S. Yehezkel, M. Auinat, N. Sezin, D. Starosvetsky, Y. Ein-Eli, Bundled and densified carbon nanotubes (CNT) fabrics as flexible ultra-light weight li-ion battery anode current collectors, *J. Power Sources* 312 (2016) 109–115.
- [6] M.F.L. De Volder, S.H. Tawfik, R.H. Baughman, A.J. Hart, Carbon nanotubes: present and future commercial applications, *Science* 80 (339) (2013) 535–539, <http://dx.doi.org/10.1126/science.1222453>.
- [7] M.J. Schulz, G. Hou, V. Ng, M. Rabiee, M. Cahay, S. Chaudhary, D. Lindley, D. Chauhan, M. Paine, D. Vijayakumar, C. Xu, Z. Yin, K. Haworth, Y. Liu, M. Sundaram, W. Li, D. Mast, V.N. Shanov, Science to Commercialization of Carbon Nanotube Sheet and Yarn, 12, 2017 41–50.
- [8] M.J. Schulz, B. Ruff, A. Johnson, K. Vemaganti, W. Li, M.M. Sundaram, G. Hou, A. Krishnaswamy, G. Li, S. Fialkova, S. Yarmolenko, A. Wang, Y. Liu, J. Sullivan, N. Alvarez, V. Shanov, S. Pixley, New applications and techniques for nanotube superfiber development, *Nanotub. Superfiber Mater. Chang. Eng. Des.* (2013) 33–59, <http://dx.doi.org/10.1016/B978-1-4557-7863-8.00002-5>.
- [9] T. Gspann, F. Smail, A. Windle, Spinning of carbon nanotube fibres using the floating catalyst high temperature route: purity issues and the critical role of sulphur, *Faraday Discuss.* 173 (2014) 2–7, <http://dx.doi.org/10.1039/C4FD00066H>.
- [10] C. Paukner, K.K.K. Koziol, Ultra-pure single wall carbon nanotube fibres continuously spun without promoter, *Sci Rep* 4 (2014) 3903, <http://dx.doi.org/10.1038/srep03903>.

- [11] J.N. Wang, X.G. Luo, T. Wu, Y. Chen, High-strength carbon nanotube fibre-like ribbon with high ductility and high electrical conductivity, *Nat. Commun.* 5 (2014) 3848, <http://dx.doi.org/10.1038/ncomms4848>.
- [12] S.-H. Lee, J. Park, H.-R. Kim, T. Lee, J. Lee, Y.-O. Im, C.-H. Lee, H. Cho, H. Lee, C.-H. Jun, Y.-C. Ahn, I.-B. Lee, K.-H. Lee, Synthesis of carbon nanotube fibers using the direct spinning process based on Design of Experiment (DOE), *Carbon N. Y.* 100 (2016) 647–655, <http://dx.doi.org/10.1016/j.carbon.2016.01.034>.
- [13] G. Hou, V. Ng, Y. Song, L. Zhang, C. Xu, V. Shanov, D. Mast, M. Schulz, Y. Liu, Numerical and experimental investigation of carbon nanotube sock formation, *MRS Adv.* (2016) 1–6, <http://dx.doi.org/10.1557/adv.2016.632>.
- [14] P. Liu, Y.F. Tan, D.C.M.M. Hu, D. Jewell, H.M. Duong, Multi-property enhancement of aligned carbon nanotube-epoxy thin film composites, *Mater. Des.* 108 (2016) 754–760, <http://dx.doi.org/10.1016/j.matdes.2016.07.045>.
- [15] P. Liu, A. Lam, Z. Fan, T.Q. Tran, H.M. Duong, Advanced multifunctional properties of aligned carbon nanotube-epoxy thin film composites, *Mater. Des.* 87 (2015) 600–605, <http://dx.doi.org/10.1016/j.matdes.2015.08.068>.
- [16] M.W. Schauer, M.A. White, Tailoring industrial scale CNT production to specialty markets, *MRS Proc.* 1752 (2015) mrsf14-1752-mm04-07, <http://dx.doi.org/10.1557/opl.2015.90>.
- [17] M.W. Schauer, D.S. Lashmore, D.J. Lewis, B.M. Lewis, E.C. Towle, Strength and electrical conductivity of carbon nanotube yarns, *Mater. Res.* 1258 (2010).
- [18] K.K.K. Koziol, C. Ducati, A.H. Windle, Carbon nanotubes with catalyst controlled chiral angle, *Chem. Mater.* 22 (2010) 4904–4911, <http://dx.doi.org/10.1021/cm100916m>.
- [19] S.W. Pattinson, K. Prehn, I.A. Kinloch, D. Eder, K.K.K. Koziol, K. Schulte, A.H. Windle, The life and death of carbon nanotubes, *RSC Adv.* 2 (2012) 2909, <http://dx.doi.org/10.1039/c2ra00660j>.
- [20] G. Hou, R. Su, A. Wang, V. Ng, W. Li, Y. Song, L. Zhang, M. Sundaram, V. Shanov, D. Mast, D. Lashmore, M. Schulz, Y. Liu, The effect of a convection vortex on sock formation in the floating catalyst method for carbon nanotube synthesis, *Carbon N. Y.* 102 (2016) 513–519, <http://dx.doi.org/10.1016/j.carbon.2016.02.087>.
- [21] G. Hou, V. Ng, C. Xu, L. Zhang, G. Zhang, V. Shanov, D. Mast, W. Kim, M. Schulz, Y. Liu, Multiscale modeling of carbon nanotube bundle agglomeration inside a gas phase pyrolysis reactor, *MRS Adv.* (2017) 1–6, <http://dx.doi.org/10.1557/adv.2017.371>.
- [22] T.S. Gspann, S.M. Juckes, J.F. Niven, M.B. Johnson, J.A. Elliott, M.A. White, A.H. Windle, High thermal conductivities of carbon nanotube films and micro-fibres and their dependence on morphology, *Carbon N. Y.* 114 (2016) 160–168, <http://dx.doi.org/10.1016/j.carbon.2016.12.006>.
- [23] M. Monthieux, P. Serp, E. Flahaut, M. Razafinimanana, C. Laurent, A. Peigney, W. Bacsa, J.-M. Broto, Introduction to carbon nanotubes, *Springer Handb. Nanotechnol.*, Springer 2007, pp. 43–112.
- [24] Q. Liu, W. Ren, F. Li, H. Cong, H.-M. Cheng, Synthesis and high thermal stability of double-walled carbon nanotubes using nickel formate dihydrate as catalyst precursor, *J. Phys. Chem. C* 111 (2007) 5006–5013, <http://dx.doi.org/10.1021/jp068672k>.
- [25] T. Guo, P. Nikolaev, A.G. Rinzler, D. Tomanek, D.T. Colbert, R.E. Smalley, Self-assembly of tubular fullerenes, *J. Phys. Chem.* 99 (1995) 10694–10697, <http://dx.doi.org/10.1021/j100027a002>.
- [26] Q. Zhang, J.-Q. Huang, M.-Q. Zhao, W.-Z. Qian, F. Wei, Modulating the diameter of carbon nanotubes in array form via floating catalyst chemical vapor deposition, *Appl. Phys. A Mater. Sci. Process.* 94 (2009) 853–860, <http://dx.doi.org/10.1007/s00339-008-4904-5>.
- [27] C. Singh, M.S.P. Shaffer, A.H. Windle, Production of controlled architectures of aligned carbon nanotubes by an injection chemical vapour deposition method, *Carbon N. Y.* 41 (2003) 359–368, [http://dx.doi.org/10.1016/S0008-6223\(02\)00314-7](http://dx.doi.org/10.1016/S0008-6223(02)00314-7).
- [28] K.-E. Kim, K.-J. Kim, W.S. Jung, S.Y. Bae, J. Park, J. Choi, J. Choo, Investigation on the temperature-dependent growth rate of carbon nanotubes using chemical vapor deposition of ferrocene and acetylene, *Chem. Phys. Lett.* 401 (2005) 459–464, <http://dx.doi.org/10.1016/j.cplett.2004.11.113>.
- [29] R. Xiang, G. Luo, Z. Yang, Q. Zhang, W. Qian, F. Wei, Temperature effect on the substrate selectivity of carbon nanotube growth in floating chemical vapor deposition, *Nanotechnology* 18 (2007) 415703, <http://dx.doi.org/10.1088/0957-4484/18/41/415703>.
- [30] J.J. Vilatela, A.H. Windle, Yarn-like carbon nanotube fibers, *Adv. Mater.* 22 (2010) 4959–4963, <http://dx.doi.org/10.1002/adma.201002131>.
- [31] X.-H. Zhong, Y.-L. Li, J.-M. Feng, Y.-R. Kang, S.-S. Han, Fabrication of a multifunctional carbon nanotube “cotton” yarn by the direct chemical vapor deposition spinning process, *Nano* 4 (2012) 5614, <http://dx.doi.org/10.1039/c2nr31309j>.
- [32] B. Alemán, M.M. Bernal, B. Mas, E.M. Perez, V. Reguero, G. Xu, Y. Cui, J. Vilatela, Inherent predominance of high chiral angle metallic carbon nanotubes in continuous fibers grown from molten catalyst, *Nanoscale* (2016) <http://dx.doi.org/10.1039/C5NR07455J>.
- [33] E. Senokos, V. Reguero, J. Palma, J. Vilatela, R. Marcilla, Macroscopic fibres of CNTs as electrodes for multifunctional electric double layer capacitors: from quantum capacitance to device performance, *Nanoscale* (2016) <http://dx.doi.org/10.1039/C5NR07697H>.
- [34] J. Terrones, J.A. Elliott, J.J. Vilatela, A.H. Windle, Electric field-modulated non-ohmic behavior of carbon nanotube fibers in polar liquids, *ACS Nano* (2014) 8497–8504, <http://dx.doi.org/10.1021/nn5030835>.
- [35] C. Hoecker, F. Smail, M. Bajada, M. Pick, A. Boies, Catalyst nanoparticle growth dynamics and their influence on product morphology in a CVD process for continuous carbon nanotube synthesis, *Carbon N. Y.* (2015) <http://dx.doi.org/10.1016/j.carbon.2015.09.050>.
- [36] V. Reguero, B. Alemán, B. Mas, J.J. Vilatela, Controlling carbon nanotube type in macroscopic fibers synthesized by the direct spinning process, *Chem. Mater.* 26 (2014) 3550–3557, <http://dx.doi.org/10.1021/cm501187x>.
- [37] S. Boncel, R.M. Sundaram, A.H. Windle, K.K.K. Koziol, Enhancement of the mechanical properties of directly spun CNT fibers by chemical treatment, *ACS Nano* 5 (2011) 9339–9344, <http://dx.doi.org/10.1021/nn202685x>.
- [38] K.L. Stano, K. Koziol, M. Pick, M.S. Motta, A. Moiala, J.J. Vilatela, S. Frasier, A.H. Windle, Direct spinning of carbon nanotube fibers from liquid feedstock, *Int. J. Mater. Form.* 1 (2008) 59–62, <http://dx.doi.org/10.1007/s12289-008-0380-x>.
- [39] M. Motta, A. Moiala, I.A. Kinloch, A.H. Windle, High performance fibres from “dog bone” carbon nanotubes, *Adv. Mater.* 19 (2007) 3721–3726, <http://dx.doi.org/10.1002/adma.200700516>.
- [40] D. Conroy, A. Moiala, S. Cardoso, A. Windle, J. Davidson, Carbon nanotube reactor: ferrocene decomposition, iron particle growth, nanotube aggregation and scale-up, *Chem. Eng. Sci.* 65 (2010) 2965–2977, <http://dx.doi.org/10.1016/j.ces.2010.01.019>.
- [41] A. Windle, Carbon nanotube fibres: science and technology transfer, in: A. Misra, J.R. Bellare (Eds.), *Nanosci. Technol. Mank*, The National Academy of Sciences, India, 2014 10.1.1.731.4910.
- [42] T.S. Gspann, N. Montinaro, A. Pantano, J.A. Elliott, A.H. Windle, Mechanical properties of carbon nanotube fibres: St Venant’s principle at the limit and the role of imperfections, *Carbon N. Y.* 93 (2015) 1021–1033, <http://dx.doi.org/10.1016/j.carbon.2015.05.065>.
- [43] P. Davies, P. Papakonstantinou, N. Martin, I. Kratochvílová, C. Ewels, M. Shaffer, T. Enoki, M. Heggge, T. Gspann, A. Turak, O.A. Bårnsan, D. Zitoun, P. Ajayan, L. Mooring, V. Khare, A. Zöpfl, A. Hirsch, M. Baxendale, P. Costa, V. Falko, J. Casado, L.S. Hui, A. Windle, A. Sinititskii, M. Rosseinsky, T. Nguyen, Synthesis in gas and liquid phase: general discussion, *Faraday Discuss.* 173 (2014) 115–135, <http://dx.doi.org/10.1039/C4FD90042A>.